Assessing CO, NO_2, And SO_2 Levels and Urban Heat Island Dynamics in the Caraga Region, Philippines Through Remote Sensing

Jun Love E. Gesta
Department of Geodetic Engineering, College of Engineering and Geosciences, Caraga State University

Kim Lyra D. Mateo
Department of Geodetic Engineering, College of Engineering and Geosciences, Caraga State University

Nathaniel G. Radaza
Department of Geodetic Engineering, College of Engineering and Geosciences, Caraga State University

https://doi.org/10.5109/7323417

出版情報：Proceedings of International Exchange and Innovation Conference on Engineering & Sciences (IEICES). 10, pp.1255-1262, 2024-10-17. International Exchange and Innovation Conference on Engineering & Sciences
バージョン：

Assessing CO, NO_2, and SO_2 Levels and Urban Heat Island Dynamics in the Caraga Region, Philippines Through Remote Sensing

Jun Love E. Gesta[1,2], Kim Lyra D. Mateo[1], Nathaniel G. Radaza[1]
[1]Department of Geodetic Engineering, [2]Caraga Center for Geo-Informatics,
College of Engineering and Geosciences, Caraga State University, Butuan City, 8600, Philippines
Corresponding author email: jlegesta@carsu.edu.ph

Abstract: *Swift urban growth in the Caraga region has intensified land use changes, city morphology alterations, and heat emissions, forming urban heat islands (UHI) and increasing air pollution. This study aims to assess UHI dynamics and their relationship with Carbon monoxide (CO), Sulphur dioxide (SO_2), Nitrogen dioxide (NO_2) levels in the region. Using Landsat 8 satellite data from 2013-2023 and Sentinel-5P data from 2019-2023, the study determined UHI and air pollutant levels. Among Caraga's significant cities, Butuan City exhibited consistently higher UHI values and the most extensive UHI. By employing Spearman's correlation coefficient, results suggest CO levels have a more consistent positive correlation with UHI across the cities, except for Bayugan City, compared to NO_2 and SO_2. The geographical location of Bayugan City might explain this finding, as it is the only one among the five cities not situated along the coast and is bordered by mountainous areas.*

Keywords: urban heat island, Carbon monoxide (CO), Sulphur dioxide (SO_2), Nitrogen dioxide (NO_2), air pollutants

1. INTRODUCTION

Urban heat islands (UHIs) are regions within urbanized areas that register higher temperatures compared to the surrounding non-urban regions [1]. Additionally, the acceleration of urbanization plays a role in the urban heat island effect, where urban areas experience higher temperatures than nearby rural areas. This rapid increase in urbanization has been driven by limited resources, rising pollution, and the necessity for urban economic transformation [2]. This occurs because built structures absorb and hold onto heat, exacerbating temperature differences, as stated by Ciu et al. [3]. The prevalence of UHI in major cities is mainly attributed to urban development and heightened vehicular emissions. The effect of UHI significantly impacts the daily lives of urban dwellers and can amplify the threat of heat-related fatalities linked to global climate shifts [4]. The Caraga region in the northeastern part of Mindanao, Philippines, is experiencing swift urban growth and industrial expansion. This rapid development has brought about more traffic, industrial operations, and higher population density, which has sparked worries about air pollution and the UHI phenomenon in the area.

According to Ngarambe et al. [5], the rapid growth of urban populations leads to heightened human activities, including the burning of fossil fuels for transportation, cooking, and climate control in buildings. This surge results in elevated levels of air pollutants such as Sulphur dioxide (SO_2), Nitrogen dioxide (NO_2), and Carbon monoxide (CO), posing significant risks to both human health and the environment [6,7]. It is crucial to grasp the spatial and temporal distribution of these pollutants and their relationship with UHI phenomena to develop effective strategies for mitigation and urban planning policies. Utilizing remote sensing technologies and geospatial analysis tools like Google Earth Engine (GEE) offers an opportunity to comprehensively evaluate UHI dynamics at both regional and local levels [8].

Landsat 8, jointly operated by the U.S. Geological Survey (USGS) and NASA, constitutes a multispectral satellite mission delivering moderate spatial resolution images of the Earth's surface. This satellite hosts the Operational Land Imager (OLI) and the Thermal Infrared Sensor (TIRS) instruments. The OLI captures data across the visible, near-infrared, and shortwave infrared portions of the spectrum, while the TIRS measures land surface temperature utilizing advanced quantum physics principles [9,10]. Specifically, the Thermal Infrared Sensor (TIRS) on Landsat 8 furnishes crucial data on land surface temperature (LST), which is essential for investigating urban heat island effects [11].

On the other hand, the Tropospheric Monitoring Instrument (TROPOMI), installed on the Copernicus Sentinel-5 Precursor satellite, marks a significant leap in atmospheric monitoring capabilities. This space-borne spectrometer, with a nadir-viewing configuration, covers wavelengths from ultraviolet to shortwave infrared [12]. TROPOMI serves as the primary payload on ESA's Sentinel-5P spacecraft, capturing solar radiation reflected by and emitted from Earth, enabling the retrieval of essential atmospheric parameters such as CO, NO_2, and SO_2 concentrations [13].

This study employs Landsat 8 imagery to assess the urban heat island effect in the Caraga region. By analyzing temperature disparities between urban and rural zones, researchers can identify and measure the extent of the urban heat island phenomenon. Combining Landsat 8 data with TROPOMI measurements facilitates a thorough examination of the correlation between air pollutant concentrations and UHI dynamics. Such analysis yields valuable insights crucial for fostering sustainable urban development and effective environmental management practices in the region.

2. METHODOLOGY

This chapter outlines a comprehensive methodology for extracting urban heat island (UHI) and pollutant concentrations (CO, SO_2, and NO_2) from Landsat 8 and

Sentinel 5P satellite imagery, respectively, utilizing Google Earth Engine. The approach encompasses several crucial steps for Landsat 8 datasets, such as converting digital numbers to radiance and brightness temperature, estimating land surface emissivity using spectral indices, and quantifying UHI values via threshold calculations.

2.1 Study Area

Caraga is a region situated in the northeastern part of Mindanao, Philippines, and comprised of five provinces: Agusan del Norte, Agusan del Sur, Surigao del Norte, Surigao del Sur, and Dinagat Islands. Additionally, the region includes six cities: Bayugan, Bislig, Butuan, Cabadbaran, Surigao, and Tandag, along with 67 municipalities and 1,311 barangays. The total land area of Caraga spans 1,913,842 hectares, accommodating a population of 2,596,709 with a population growth rate of 1.28% and a population density of 136 persons/ km^2, as of 2015 [14].

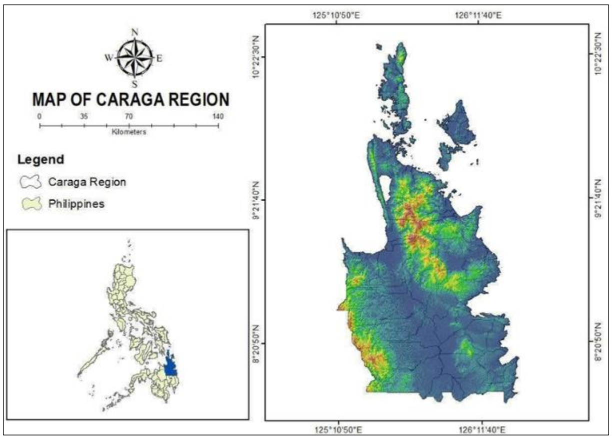

Fig. 1. Map of Caraga region.

2.2 Data acquisition

The United States Geological Survey (USGS) provides Top of Atmosphere (TOA) brightness temperatures for the thermal infrared (TIR) channels of Landsat satellites. Landsat 8's Operational Land Imager (OLI) captures data in the visible and short-wave infrared range, while the Thermal Infrared Sensor (TIRS) provides the TIR data. These data are readily accessible and well-suited for utilization within the GEE platform for Landsat 8, collection 2. TOA values are derived by the USGS from raw orthorectified digital numbers of data using the respective calibration coefficients [15]. The Landsat series data are considered consistent and inter-calibrated, with all TIR bands resampled to a 30-meter spatial resolution. Table 1 outlines the properties of the spectral bands utilized in this study for Landsat 8. In addition to the TIR band, the red and near-infrared (NIR) bands are used to derive the Normalized Difference Vegetation Index (NDVI), calculated from the Surface Reflectance (SR) values instead of the TOA values, which are less accurate.

This study used Landsat 8 satellite imagery to assess the UHI, while Sentinel-5p satellite images were used for analyzing CO, NO_2, and SO_2 levels in the region. Google has developed GEE as a cloud computing platform to effectively address the challenges associated with extensive data analysis. This platform facilitates the acquisition of datasets and processing of large geodatasets over vast areas and allows for the long-term monitoring of the environment [16].

Table 1. Properties of the spectral bands utilized in this study for Landsat 8

Satellite	Used Bands	Wavelength (μm)	Spatial resolution
Landsat 8 (OLI; TIRS)	SR_B4	0.64-0.67	30 m
	SR_ B5	0.85-0.88	30 m
	SR_B10	10.6-11.9	100^2 m

2.3 Extraction of UHI, CO, SO_2, and NO_2 data

2.3.1 Top of Atmosphere (TOA) spectral radiance

Top of Atmosphere (TOA) Reflectance is a dimensionless measurement that represents the ratio of radiation reflected from the surface to the incident solar radiation. The Landsat Thematic Mapper (TM) and Enhanced Thematic Mapper Plus (ETM+) sensors capture this reflected solar energy. The raw dataset was converted to TOA spectral radiance using the radiance rescaling factors in the MTL file using equation (1) [17].

$$L\lambda = ML*Qcal + AL \quad (1)$$

Where:

$L\lambda$ = TOA spectral radiance (Watts/ m2 * sr * μm)
ML = Radiance multiplicative Band (No.)
Qcal = Quantized and calibrated standard product pixel values (DN)
AL = Radiance Add Band (No.)

2.3.2 Conversion of radiance ($L\lambda$) to brightness temperature (BT)

Thermal band data can indeed be converted from spectral radiance to top of atmosphere brightness temperature (BT) using equation (2), as outlined by the United States Geological Survey [18].

$$BT= K2 / \ln (K1 / L\lambda + 1) - 273.15 \quad (2)$$

Where:

BT = Top of atmospheric brightness temperature (°C)
K1 = Constant Band (No.)
K2 = Constant Band (No.)

2.3.3 Land Surface Emissivity (LSE)

Emissivity refers to the ability of a material to influence thermal conditions by determining the reflectance and absorption of solar energy [19]. The emissivity of land surfaces varies depending on factors such as vegetation density, land moisture content, surface roughness, and the angle at which energy interacts with the surface. The evaluation of land surface emissivity (ε) values can be conducted using methods such as the Normalized Difference Vegetation Index (NDVI) and the Proportion Vegetation (PV) method [20].

$$\varepsilon = 0.004 * Pv + 0.986 \quad (3)$$

$$PV = \left(\frac{NDVI-NDVImin}{NDVImax-NDVImin}\right)^2 \quad (4)$$

$$\text{NDVI} = \frac{(\text{NIR band} - \text{Red band})}{(\text{NIR band} + \text{Red band})} \quad (5)$$

Where:

PV = Proportion vegetation
NDVI = DN values from NDVI Image
NDVI min = Minimum DN values from NDVI Image
NDVI max = Maximum DN values from NDVI Image
RED = DN values from the RED band
NIR = DN values from the Near-Infrared band

2.3.4 Land Surface Temperature (LST)

Land surface temperature (LST) is a crucial indicator used to measure the radiative skin temperature of the Earth's surface, derived from infrared radiation. It plays a significant role in energy cycles, ecological system balance, and human life [20]. Equation (6) was utilized to compute the LST.

$$\text{LST} = \text{BT}/\ (1+\lambda*\text{BT}/c2)\ *\ln(\varepsilon) \quad (6)$$

Where:

λ = effective wavelength (Band Thermal)
C2 = h*c/s= $1.4338*10^{-2}$mK = 14338MK
S = s is Boltzmann constant value ($1{,}38 \times 10^{-23}$ JK^{-1})
C = light speed in vacuum ($2{,}998 \times 10^{-8}$ Ms^{-1})

2.3.5 Urban heat island (UHI)

The urban heat island (UHI) phenomenon is typically divided into two components: Land UHI and atmospheric UHI. Remote sensing techniques primarily capture and quantify the Land UHI, which visualizes the temperature disparities caused by land surface temperatures compared to air temperatures [21]. Using equation (7), the UHI value is calculated from LST data using threshold calculations to delineate and characterize areas experiencing significant UHI effects.

$$\text{UHI} = \text{Ts} - \text{Tm}\ /\text{Tst} \quad (7)$$

Where:

Ts = Land surface temperature value
Tmean = mean value of Land surface temperature
Tstd = standard deviation of land surface temperature value

UHI calculation used a threshold calculation to see if a positive value represented the UHI and a value lower than 0 represented no UHI in the [21].

2.3.6 Extraction of Sentinel 5P NRTI data using Google Earth Engine

A Google Earth Engine script was employed to retrieve Carbon Monoxide (CO), Nitrogen Dioxide (NO_2), and Sulfur Dioxide (SO_2) concentration data from the Copernicus Sentinel-5P satellite. Different scripts facilitated the selection of each pollutant's column number density images, filtering them by date and location, and clipping them to a specified region.

2.4 Spearman's Correlation Coefficient

Spearman's rank correlation coefficient is a statistical measure that shows the strength of a monotonic relationship between two variables [22]. Spearman's correlation coefficient is applied to a sample using the equation (8):

$$r_s = 1 - \frac{6\sum d_i^2}{n^3 - n} \quad (8)$$

Where:

d_i = difference in ranks of *i*th observation for sample 1 and sample 2
n = number of pairs of observations

The validity will be interpreted using the categorization in Table 2. This descriptor applies to both positive and negative relationships [23].

Table 2. Interpretation table of Spearman Rank-Order Correlation Coefficients

Spearman (r_s)	Correlation
≥ 0.70	Very strong relationship
0.40-0.69	Strong relationship
0.30-0.39	Moderate relationship
0.20-0.29	Weak relationship
0.01-0.19	Negligible relationship

3. RESULTS AND DISCUSSIONS

3.1 Land Surface Temperature

The study conducted in the Caraga region thoroughly assessed the fluctuations in LST over a significant duration spanning from 2013 to 2023, employing advanced time series analysis tools to analyze the variations in the LST dataset meticulously. It noted the division of time into two semi-annual periods, January to June and July to December, which aids in better trend analysis and ensures a more consistent temporal resolution for the images used in the study. This segmentation allows for a detailed examination of LST trends within each period, facilitating the identification of variations and patterns critical for understanding surface temperature dynamics.

The LST for January to June (shown in Fig. 2) in the Caraga region exhibits notable variability over the years, as evidenced by the data provided. In 2013, the mean LST stood at 23.23°C, with a maximum of 36.4°C and a minimum of 15.17°C, marking a moderate temperature. Subsequent years experienced swings, with 2015 posting the highest January to June LST of 25.63°C, with a maximum of 38.3°C and a minimum of 18.69°C, indicating much warmer temperatures. However, 2018 marked a notable decrease, with temperatures dropping to 21.27°C, with a maximum of 32.15°C and a minimum of 13.6°C, suggesting more excellent conditions than earlier. This trend shifted again in 2019, with mean LST rising to 24.48°C, with a maximum of 35.28°C and a minimum of 19.41°C, indicating a return to warmer conditions. Notably, 2022 and 2023 experienced remarkable increases in January to June LST, reaching an average temperature of 27.31°C and 30.46°C, respectively, indicating hot conditions.

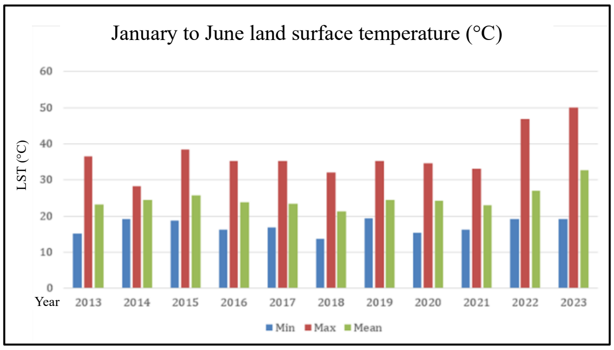

Fig. 2. Trend of the January to June land surface temperature in the Caraga region.

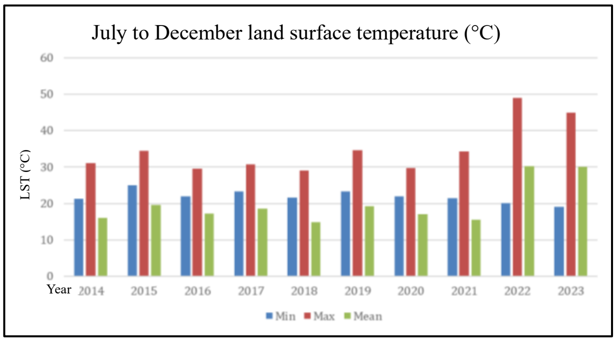

Fig. 3. Trend of the July to December land surface temperature in the Caraga region.

The LST for July to December (shown in Fig. 3) in the Caraga region from 2013 to 2023 offers valuable insights into the temperature dynamics over the years. In 2013, the LST ranged from a minimum of 10.85°C to a maximum of 32.96°C, resulting in a mean temperature of 19.74°C. This was followed by a slight increase in both minimum and maximum LST values in 2014, ranging from 16.07°C to 31.06°C, leading to a higher mean LST of 21.22°C. However, 2015 witnessed a substantial rise in temperatures, with the minimum reaching 19.64°C and the maximum soaring to 34.47°C, contributing to a notable increase in the mean LST to 25.07°C. Despite fluctuations in minimum and maximum temperatures from 2016 to 2018, the mean LST remained relatively stable, ranging from 21.56°C to 23.26°C. In 2019, there was a noteworthy increase in mean LST to 23.28°C, signaling a return to warmer conditions. The years 2020 and 2021 displayed mean LST values like previous years. However, the most significant observation was in 2022 and 2023, which exhibited remarkably higher mean LST values of 27.01°C and 29.33°C, respectively, indicating a significant warming trend.

3.2 Urban heat island in significant cities of the Caraga region

A comprehensive evaluation of changes in UHI dynamics from 2013 to 2023 in the Caraga region was focused on its five significant cities: Butuan, Surigao, Tandag, Bayugan, and Bislig City. Complex fluctuations in the UHI dataset were observed across this period using advanced time series analysis techniques. Recognizing the semi-annual nature of the region's UHI patterns, the study delineated two distinct periods: January to June and July to December. This division aids in capturing the different variations in UHI dynamics throughout the year, providing valuable insights into how urban heat islands evolve.

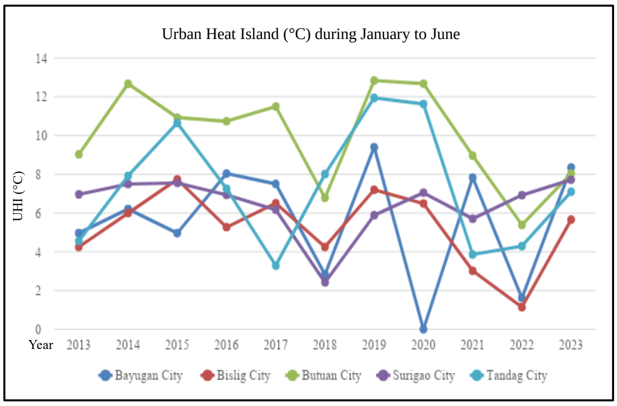

Fig. 4. Trend of the urban heat island during January to June in all significant cities in the Caraga region.

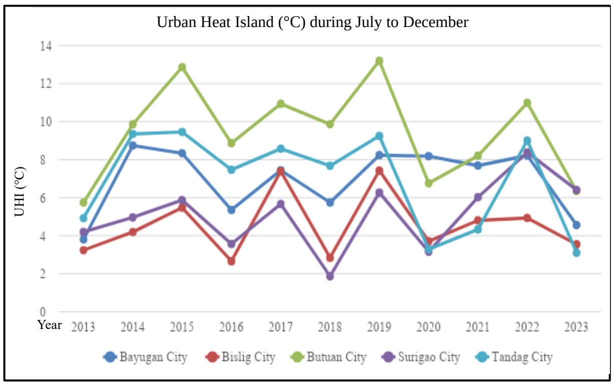

Fig. 5. Trend of the urban heat island during July to December in all significant cities in the Caraga region.

As observed in Fig. 4, Butuan City recorded the highest UHI in 2014. With a UHI value of 12.68°C, Butuan City experienced a considerable temperature difference between its urban and rural areas. Throughout 2015, Butuan City continued to have the highest UHI, with a UHI value of 10.93°C, indicating enduring urban heat island effects. Following this trend, Butuan City maintained the highest UHI in 2016. The city's UHI value of 10.74°C in 2017 highlights the continuing impact of urban heat islands. Butuan City exhibited the highest UHIs in 2018, 2019, 2020, 2021, 2022, and 2023, implying that the effect of UHI in the city is more apparent than in the other major cities. From July to December 2013 (shown in Fig. 5), Butuan City still showed the highest UHI effect with a value of 5.75°C, showcasing a noticeable difference from its neighboring areas. This trend continued into 2014 when Butuan City maintained its position with the highest UHI. The city experienced a significant temperature disparity between its urban and rural zones, recording a UHI value of 9.86°C. Throughout 2015, Butuan City consistently displayed the highest UHI, with a value of 12.87°C, indicating persistent urban heat island effects. This pattern persisted in 2016, 2017, 2018, 2019, 2020, 2021, 2022, and 2023.

3.3 Extent of urban heat island in significant cities

The extent of urban heat island in square kilometers (sq.km) for each city during January to June shows that Butuan City has the largest area of UHI effect among the five cities, ranging from 310.19 sq.km in 2013 to 323.19

sq.km in 2023. On the other hand, the extent of UHI in Bislig City and Surigao City have an area ranging from 106.11 sq.km to 128.64 sq.km and 115.81 sq.km to 128.64 sq.km, respectively. Similarly, Bayugan and Tandag City have experienced fluctuations in their UHI, indicating possible changes in land use patterns.

The analysis of the UHI effect across five cities reveals distinct patterns of urbanization and land use changes, particularly evident during the month of July to December. Among the cities, Butuan City consistently exhibits the largest UHI area. The expansion of Butuan's UHI area from 301.33 sq.km in 2013 to 394.26 sq.km in 2023 signifies a notable increase in urban development and land transformation. Bislig City and Surigao City also experience considerable UHI effects, with fluctuating UHI areas ranging from 203.06 sq.km to 276.22 sq.km and 117.86 sq.km to 174.58 sq.km, respectively, during July to December. The same with other cities, Bayugan and Tandag exhibits fluctuations in UHI, possibly influenced by environmental factors and developmental activities.

3.4 CO, NO_2, and SO_2 Emission in Significant Cities of Caraga Region

The analysis of CO, NO_2, and SO_2 emissions in the significant cities of the Caraga region from January to June reveals notable trends. In Bayugan City, the highest recorded maximum CO level was observed in 2020, reaching approximately 0.0310584 moles per square meter (mol/m^2). This peak was followed by fluctuations in subsequent years, with the lowest maximum CO level noted in 2022 at approximately 0.02683305 mol/m^2. Moving to NO_2 emissions, the highest maximum level in Bayugan City occurred in 2023, at approximately 0.000043866 mol/m^2, marking an increase over the years analyzed. Similarly, SO_2 emissions in Bayugan City reached their highest maximum in 2022, at approximately 0.000237401 mol/m^2, showcasing significant variability compared to other years.

In Bislig City, the highest maximum CO level was recorded in 2019, at approximately 0.0307315 mol/m^2, with subsequent years showing decreasing trends. For NO_2 in Bislig City, the peak maximum occurred in 2022, at approximately 0.0000428972 mol/m^2, while SO_2 levels peaked in 2020, reaching approximately 0.00019289 mol/m^2. Butuan City experienced its highest maximum CO level in 2019, at approximately 0.0319045 mol/m^2, with reductions in subsequent years. The highest maximum NO_2 level in Butuan City was recorded in 2023, at approximately 0.000044624 mol/m^2, whereas SO_2 emissions peaked in 2022, at approximately 0.000154913 mol/m^2.

Surigao City observed the highest maximum CO level in 2020, at approximately 0.0386025 mol/m^2, showcasing fluctuations over the years. The highest maximum NO_2 level in Surigao City occurred in 2023, at approximately 0.0000457341 mol/m^2, while SO_2 emissions peaked in 2019 at approximately 0.000108711 mol/m^2. Lastly, the highest recorded maximum CO level in Tandag City occurred in 2021, reaching approximately 0.0342907 mol/m^2, showing fluctuations in subsequent years, with the lowest maximum CO level noted in 2023 at approximately 0.0287177 mol/m^2. Moving to NO_2 emissions, the highest maximum level in Tandag City was observed in 2020, at approximately 0.0000451232 mol/m^2, with varying levels in other years. Similarly, SO_2 emissions in Tandag City reached their highest maximum in 2022, at approximately 0.000216909 mol/m^2, showing notable variability compared to other years. These findings underscore the variability and trends in air pollutant emissions across the Caraga region.

3.5 Spearman's correlation coefficient analysis

The correlation values indicate the relationship between the UHI and air pollutant variables based on the interpretation table of Spearman rank-order correlation coefficients. Additionally, the p-value will determine whether the hypothesis results are statistically significant ($p < 0.05$). In Bayugan City (shown in Table 3), a positive negligible relationship was observed between UHI and CO, with a correlation value of 0.05 and a p-value of 0.737. This result is insignificant and indicates a minimal influence of CO on UHI intensity. Similarly, UHI showed positive negligible relationships with both NO_2, with a correlation value of 0.14 and p-value of 0.328, and SO_2, with a correlation value of 0.14 and p-value of 0.321, with the results being insignificant and suggesting a minimal influence of these pollutants on UHI intensity.

In contrast, in Bislig City (shown in Table 3), a positive moderate relationship was found between UHI and CO, with a correlation value of 0.38 and a p-value of 0.009 (as shown in Fig. 6b). This significant result suggests a stronger association between CO levels and UHI intensity. However, UHI exhibited positive negligible relationships with both NO_2, with a correlation value of 0.02 and a p-value of 0.889, and SO_2 with a correlation value of -0.15 and a p-value of 0.304. There are insignificant correlations between UHI and NO_2 and UHI and SO_2.

In Butuan City (shown in Table 3), a positive moderate relationship was observed between UHI and CO with a correlation value of 0.34 and p-value of 0.018, as shown in Fig. 6c. This result is significant, indicating a moderate impact of CO on UHI intensity. Conversely, UHI displayed positive negligible relationships with both NO_2 with a correlation value of 0.04 and p-value of 0.776 and SO_2 correlation value of -0.12 and p-value of 0.432, which indicates insignificant results, respectively, indicating the limited influence of these pollutants on UHI.

Similarly, in Surigao City (shown in Table 3), a positive moderate relationship was identified between UHI and CO with a correlation value of 0.36 and a p-value of 0.012, indicating a significant result and moderate association between CO levels and UHI intensity. However, UHI exhibited positive negligible relationships with NO_2, with a correlation value of 0.04 and a p-value of 0.765, and SO_2, with a correlation value of -0.03 and a p-value of 0.861, suggesting an insignificant result and minimal impact of these pollutants on UHI.

In Tandag City (shown in Table 3), a positive moderate relationship was found between UHI and CO with a correlation value of 0.30 and p-value of 0.042, indicating a significant result and moderate influence of CO on UHI intensity. Nevertheless, UHI demonstrated a positive negligible relationship with NO_2 with a correlation value of 0.08 and a p-value of 0.619, indicating an insignificant result and a negative negligible relationship with SO_2 with a correlation value of -0.23 and p-value of 0.127, suggesting an insignificant result and limited impact of these pollutants on UHI.

Table 3. Correlation values (r_s) and p-value between the UHI and air pollutants

City	Spearman (r_s)	p-value
	Carbon monoxide (CO)	
Bayugan City	0.05	0.737
Bislig City	0.38	0.009
Butuan City	0.34	0.018
Surigao City	0.36	0.012
Tandag City	0.30	0.042
	Nitrogen dioxide (NO2)	
Bayugan City	0.14	0.328
Bislig City	0.02	0.889
Butuan City	0.04	0.776
Surigao City	0.04	0.765
Tandag City	0.08	0.619
	Sulphur dioxide (SO2)	
Bayugan City	0.14	0.321
Bislig City	-0.15	0.304
Butuan City	-0.12	0.432
Surigao City	-0.03	0.861
Tandag City	-0.23	0.127

Across all cities, there is a consistent positive moderate relationship between CO and UHI except for Bayugan City; according to previous studies by Wang et al. [24], they found that the research on the relationship between UHI and air pollution varies greatly due to the difference of geographical location [24]. Also, there is a positive negligible relationship between NO_2 and UHI across all cities while SO_2 demonstrates a negative negligible relationship. Vehicular emissions and other anthropogenic activities significantly contribute to the increase in CO and NO_2 emissions, which influence the UHI effect. The consistent positive relationship implies that higher levels of CO and NO_2 coincide with increased UHI intensity, likely due to the combined heat-trapping and pollution effects of these gases in urban areas. This finding aligns with previous research by Abanzu et al. [25], indicating air pollution can intensify the urban heat island threat through high ozone concentration levels, which prevent warm air from rising and thus worsen heat island effects [25].

Conversely, SO_2 demonstrates a consistent negative negligible relationship with UHI intensity across the cities studied. SO_2 emissions primarily stem from industrial processes and fossil fuel combustion, contributing to atmospheric pollution. The negative correlation suggests that higher levels of SO_2 coincide with decreased UHI intensity.

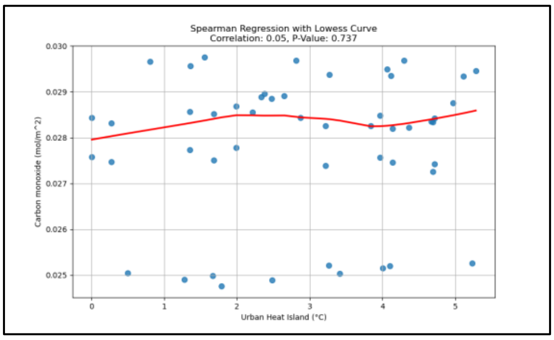

(a)

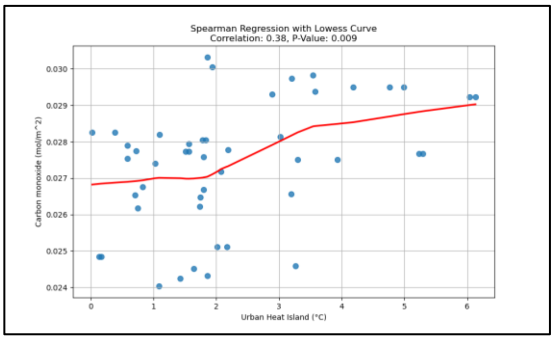

(b)

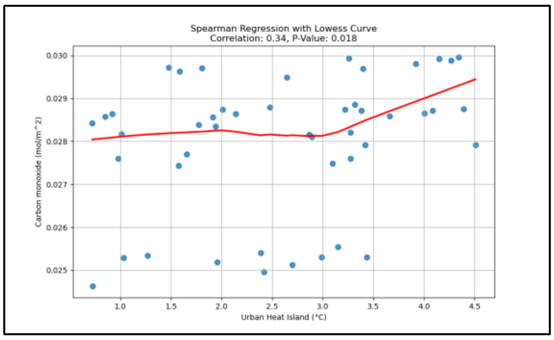

(c)

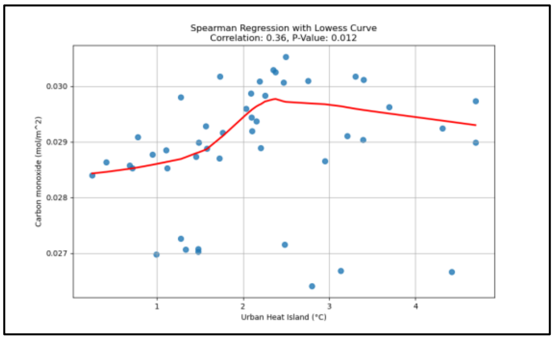

(d)

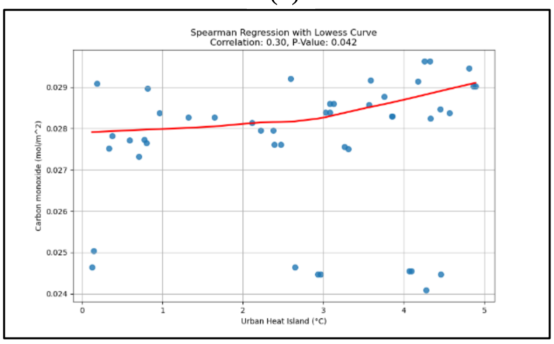

(e)

Fig. 6. Correlation analysis between UHI and CO emission in (a) Bayugan City, (b) Bislig City, (c) Butuan City, (d) Surigao City, and (e) Tandag City.

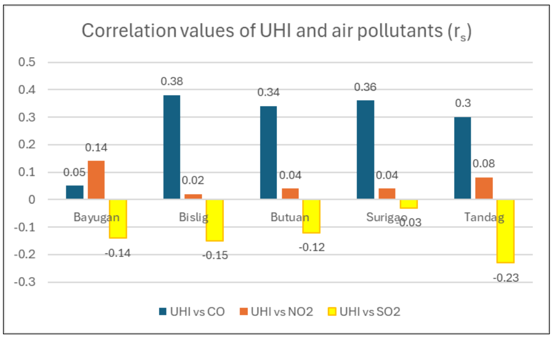

Fig. 7. Correlation values of UHI and air pollutants of significant cities in the Caraga region.

4. CONCLUSIONS AND RECOMMENDATIONS

The results show that Butuan City consistently exhibits the highest UHI effect in the Caraga Region, with significant temperature disparities between urban and rural areas over multiple years. Butuan City not only demonstrates the highest UHI intensity but also covers the largest affected area in square kilometers compared to other cities in the region. The correlation analysis, using Spearman's rank correlation coefficient, revealed a significant relationship between UHI intensity and levels of CO, NO_2, and SO_2 in the five major cities of the Caraga region. The findings highlight the significant roles of CO and NO_2 in intensifying UHI, emphasizing the need for targeted pollution control strategies to manage urban heat effectively. The CO levels showed a consistent positive moderate relationship with UHI across the cities, except for Bayugan City. The geographical location of Bayugan City might explain this finding, as it is the only one among the five cities not situated along the coast and is bordered by mountainous areas. NO_2 showed a positive negligible relationship with UHI, indicating a relatively weak impact on UHI effects. Conversely, SO_2 demonstrated a negative negligible relationship with UHI, suggesting that higher SO_2 levels might have a minor cooling effect, potentially counteracting some heat retention caused by CO and NO_2. The negligible impacts of NO_2 and SO_2 on UHI effects suggest that other factors may be more influential in these cities.

This study provides valuable insights into the complex interplay between urbanization, UHI formation, and air pollutant distribution in the Caraga region. These findings underscore the importance of targeted interventions and policy measures to mitigate UHI effects and safeguard environmental sustainability and public health in rapidly urbanizing areas. To further enhance our understanding and management of UHI effects, it is recommended to explore additional factors such as population density, road networks, and elevation on UHI intensity and spatial extent. Incorporating more air pollutants and meteorological variables into the analysis could provide a comprehensive understanding of UHI drivers.

5. REFERENCES

[1] G. El Afandi, H. Ismael, Spatiotemporal Variation of Summertime Urban Heat Island (UHI) and Its Correlation with Particulate Matter (PM2.5) over Metropolitan Cities in Alabama, Geographies, 3, 4 (2023) 622-653.

[2] V. Baskaran, R. Velkennedy, S. Murugan, G. Theerumalai, Modeling and prediction of the achievement level with related goals for SDG 11: Sustainable Cities and Communities, Proceedings of International Exchange and Innovation Conference on Engineering & Sciences (IEICES), 8 (2022) 19-24.

[3] S. Cui, Z. Song, L. Zhang, Z. Zhang, R. Hough, Q. Fu, L. An, Z. Shen, Y.-F. Li, D. Liu, S. Gao, Polycyclic aromatic hydrocarbons in fresh snow in the city of Harbin in northeast China, Atmospheric Environment, 215 (2019) Art. no. 116915.

[4] U.S. Geological Survey website: http://pubs.usgs.gov/publication/fs20213031 (accessed 27.04.24).

[5] J. Ngarambe, S. J. Joen, C.-H. Han, G. Y. Yun, Exploring the relationship between particulate matter, CO, SO2, NO2, O3 and urban heat island in Seoul, Korea, Journal of Hazardous Materials, 403 (2021) Art. no. 123615.

[6] World Health Organization (WHO) website: https://www.who.int/teams/environment-climate-change-and-health/air-quality-and-health/health-impacts/types-of-pollutants (accessed 27.04.24).

[7] S. Meo, M. Salih, F. Al-Hussain, J. Alkhalifah, A. Meo, A. Akram, Environmental pollutants PM2.5, PM10, carbon monoxide (CO), nitrogen dioxide (NO2), sulfur dioxide (SO2), and ozone (O3) impair human cognitive functions, European Review for Medical and Pharmacological Sciences, 28 (2024) 789-796.

[8] H. Shi, G. Xian, R. Auch, K. Gallo, Q. Zhou, Urban Heat Island and Its Regional Impacts Using Remotely Sensed Thermal Data—A Review of Recent Developments and Methodology, Land, 10, 8 (2021) 867.

[9] J. Storey, M. Choate, D. Moe, Landsat 8 Thermal Infrared Sensor Geometric Characterization and Calibration, Remote Sensing, 6 (2014) 11153-11181, 2014.

[10] NASA website: https://landsat.gsfc.nasa.gov/article/thermal-infrared-sensor-tirs/ (accessed 27.04.24).

[11] X. Yu, X. Guo, Z. Wu,"Land Surface Temperature Retrieval from Landsat 8 TIRS—Comparison between Radiative Transfer Equation-Based Method, Split Window Algorithm and Single Channel Method, Remote Sensing, 6 (2014) 9829-9852.

[12] TROPOMI website: https://www.tropomi.eu/ (accessed 27.04.24).

[13] B. M. Metran, J. P. Elumba, M. C. Alvardo, M. M. Bermoy, Mapping and Estimation of Road Traffic Emissions in Caraga Region using Sentinel 5P Satellite Images, Proceedings of International Exchange and Innovation Conference on Engineering & Sciences (IEICES), 9 (2023) 6-12.

[14] National Economic and Development Authority website: http://nro13.neda.gov.ph/about-caraga/ (accessed 27.04.24).

[15] Z. Qin, A. Karnieli, P. Berliner, A mono-window algorithm for retrieving land surface temperature from Landsat TM data and its application to the Israel-Egypt border region, International Journal of Remote Sensing, 22,18 (2001) 3719-3746.

[16] U.S. Geological Survey website: http://www.usgs.gov/landsat-missions/landsat-8?qt-

science_support_page_related_con=0#qt-science_support_page_related_con (accessed 27.04.24).
[17] U.S. Geological Survey website: http://www.usgs.gov/landsat-missions/using-usgs-landsat-level-1-data-product (accessed 27.04.24).
[18] Y. Yan, K. Mao, J. Shi, S. Piao, X. Shen, J. Dozier, Y. Liu, H.-L. Ren, Q. Bao, Driving forces of land surface temperature anomalous changes in North America in 2002–2018, Scientific Reports, 10 (2020) Art. no. 6931.
[19] R. Yunita, A. Wibowo, Supriatna, A. F. Rais, Urban Heat Island Mitigation Strategy based on Local Climate Zone Classification using Landsat 8 satellite imagery," IOP Conference Series: Earth and Environmental Science, 1039, 1 (2022) 012013.
[20] A. Ngie, K. Abutaleb, F. Ahmed, A. Darwish, M. Ahmed, Assessment of urban heat island using satellite remotely sensed imagery: a review, South African Geographical Journal, 96, 2 (2014) 198-214.
[21] S. Mukherjee, A. Debnath, Correlation between Land Surface Temperature and Urban Heat Island with COVID-19 in New Delhi, India, Research Square (2020).
[22] Barcelona Field Studies Centre S.L. website: https://geographyfieldwork.com/SpearmansRank.htm (accessed 27.04.24).
[23] L. Leclezio, A. Jansen, V. H. Whittemore, P. J. de Vries, Pilot validation of the tuberous sclerosis-associated neuropsychiatric disorders (TAND) checklist, Pediatric Neurology, 52, 1, (2015) 16-24.
[24] Y. Wang, Z. Guo, J. Han, The relationship between urban heat island and air pollutants and them with influencing factors in the Yangtze River Delta, China, Ecological Indicators, 129 (2021) 107976.
[25] J. Anbazu, N. S. Antwi, Nexus between heat and air pollution in urban areas and the role of resilience planning in mitigating these threats. Adv Environ Eng Res, 4 (2023) 047.